Renewable Energy 205 (2023) 1025–1039

Contents lists available at ScienceDirect

Renewable Energy

journal homepage: www.elsevier.com/locate/renene

Using vortex generators for flow separation control on tidal turbine profiles and blades

M. Manolesos [a,b,*], L. Chng [c], N. Kaufmann [d], P. Ouro [c,e], D. Ntouras [f], G. Papadakis [f]

[a] City, University of London, London, EC1V 0HB, UK
[b] Swansea University, Swansea, SA1 0NB, UK
[c] Cardiff University, Cardiff, CF10 3AT, UK
[d] Sustainable Marine, Edinburgh, EH6 6QW, UK
[e] The University of Manchester, Manchester, M13 9PL, UK
[f] National Technical University of Athens, Iroon Politechniou 9, 15780, Greece

ARTICLE INFO

Keywords:
Tidal turbines
Flow control
Vortex generators
Wind tunnel testing
RANS simulations

ABSTRACT

Tidal energy can play an important role in the Net Zero transition. Increasing tidal turbine performance through innovation is crucial if the cost of tidal energy is to become competitive compared to other sources of energy. The present investigation is a proof-of-concept study for the application of Vortex Generators (VGs) on tidal turbines in view of increasing their performance. The more mature wind energy industry uses passive VGs either as a retrofit or in the blade design process to reduce separation at the inboard part of wind turbine blades. Tidal turbine blades also experience flow separation and here we examine whether passive vane VGs can be used to reduce or suppress that separated flow. First, a wind tunnel investigation is performed to assess the performance of VGs on a 20% thick profile from the blade. Then, the VG effect on the 2D-profile is modelled in a Reynolds Averaged Navier-Stokes in-house solver. Results show that low profile VGs, i.e. VGs shorter than the local boundary layer, can increase the performance of the blade profile and successfully reduce flow separation. The VG effect on blade performance is examined in model scale and in full-size. VGs successfully suppress separation in both cases and it is shown that full-size information should be used for the placement of VGs. A maximum power coefficient increase of 1.05% is observed at a tip speed ratio of $\lambda = 3$. The present proof-of-concept study demonstrates for the first time the potential of passive VGs to be included either in the design process of a tidal turbine blade or as a retrofit solution.

1. Introduction

Vortex generators (VGs) in various forms have been used and studied for flow separation control on wings since the 1940s [1]. Their working principle is relatively simple: they generate streamwise vortices that energise the boundary layer on the surface they are attached to, by bringing high momentum fluid closer to the surface. This mechanism has been described by various researchers [2–5], while a number of studies have provided optimization guidelines under a variety of flow conditions [6–12].

It is generally accepted that vane type VGs are more effective than other passive flow control devices, such as wishbones, doublets, grooves etc [9]. Their ease of construction and implementation, robustness and light weight have made them highly popular across different industries. Examples of improved performance through the application of passive VGs include but are not limited to internal flows [10], airfoils [13], highly swept wings [14], bluff bodies [15], noise reduction [16] and horizontal axis wind turbines, either in wind tunnel tests [17,18] or in the field [19,20]. In the latter case, they are now considered a useful add-on either as a retrofit [20] or in the design phase. They are usually located at the root region of the blade, where the airfoil profiles are thicker, to limit the separation that occurs locally [21].

Horizontal axis tidal turbine blades also experience separated flow at the root region [22,23], however, investigations of VG applications on tidal turbine blades and profiles remains extremely limited. To the best of the authors' knowledge the only tidal turbine related VG study is purely computational, using a commercial Reynolds Averaged Navier Stokes (RANS) solver and does not investigate the VG sizing parameters

* Corresponding author. City, University of London, London, EC1V 0HB, UK.
E-mail address: marinos.manolesos@city.ac.uk (M. Manolesos).

https://doi.org/10.1016/j.renene.2023.02.009
Received 22 April 2022; Received in revised form 24 January 2023; Accepted 3 February 2023
Available online 7 February 2023

[24]. Furthermore, it deals with a relatively thin airfoil profile (thickness 12%), which is not representative of the root region profiles of modern tidal turbines. The other available numerical investigation [25] is by the authors' group and also uses a RANS solver to investigate VG sizing sensitivities on two hydrofoils, one 20% and one 30% thick. At the same time, in Ref. [25] a first attempt at estimating the VG effect on turbine performance was presented using low fidelity engineering tools. A maximum increase of 1.2% in power coefficient was predicted.

The present investigation aims to contribute towards filling this knowledge gap by means of a combined experimental and Computational Fluid Dynamics (CFD) investigation. The specific objectives are.

a. To explore the VG sizing parameter space in a wind tunnel for a 20% thick tidal turbine blade profile, typical of profiles used at the inner part of turbine blades
b. To use the best performing VG configuration on a turbine blade and investigate the effect on flow and performance using high fidelity computational tools and
c. To highlight the differences between model scale and full-size turbine operation with respect to VG design and placement.

The investigation concerns Schottel's SIT250 tidal turbine, a horizontal axis instream turbine with 85 kW rated mechanical power [26]. First, a 20% thick section from this blade was tested in a wind tunnel and a parametric study was performed in order to obtain a suitable vane VG configuration. The selected VG set up was then applied to the tidal turbine blade under investigation and a CFD investigation of the blade performance with and without the VGs followed. Both model scale and full-size operation was considered and the crucial differences are highlighted. The present paper is organised as follows: initially, the methodology is described, followed by the Results and Discussion section and, finally, the main findings are summarised in the concluding section.

2. Methodology

2.1. Experimental approach

The wind tunnel investigation examined a 20% thick airfoil profile, taken from the Schottel SIT250 tidal turbine blade. All experiments were performed at Swansea University's wind tunnel at a Reynolds (Re) number range $0.65 \times 10^6 \leq Re \leq 1.5 \times 10^6$ under free and fixed transition conditions. A photo of the set-up is given in Fig. 1. To fix transition, a 0.26 mm thick zigzag tape was applied across the wing span on the suction and pressure sides at chordwise positions, 0.05c and 0.10c, respectively. The test section dimensions were $1.5\,m \times 1.0\,m$ (width × height) and the free stream turbulence intensity was 0.3%. The wing spanned the wind tunnel's height, with a chord length $c = 0.5\,m$. Wind tunnel corrections for bodies spanning the tunnel test section were applied [27].

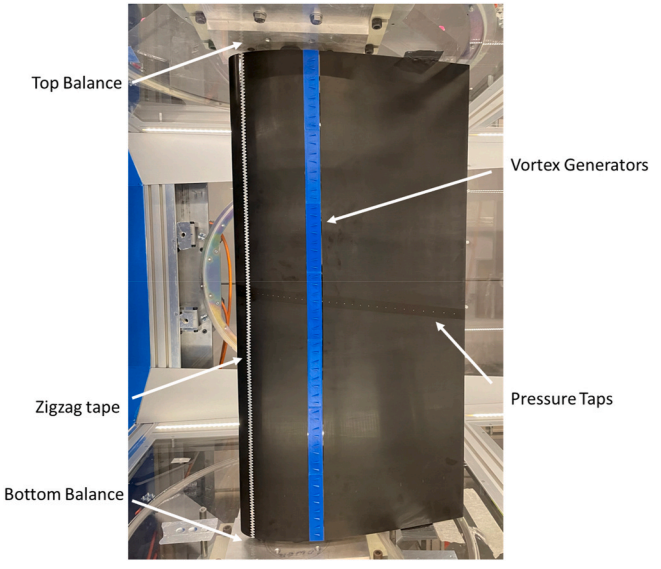

Fig. 1. The wing model inside the Swansea University Wind Tunnel test section. The flow is from left to right. The locations of the two force balances, the pressure taps, the zigzag tape and the VGs are indicated by vectors.

The extruded airfoil model was supported on two independent six-component force balances, which were recording with a sampling rate of 300 Hz for 30 s. Pressure measurements on the wing surface were performed at 10 Hz for a duration of 30 s, through 63 pressure taps connected to a Scanivalve MPS4264 64-Channel Scanner. The pressure taps extended to 95%c and all experimental lift values reported here result from the integration of the surface pressure measurements.

A second identical scanner was connected to a wake rake, which was used to measure the profile drag. The wake rake consisted of 60 total pressure tubes and 3 static pressure tubes and was located on a traverse, 1.8 chords downstream of the wing trailing edge. The traverse could move in the spanwise direction and this way the drag values at different spanwise locations could be measured. The balance measured drag was used for high angles of attack (AoA), $\alpha > \alpha_{C_{l,max}}$, where the flow is separated.

2.2. Vortex generators

Based on wind turbine literature on VG flow control [12,28], and given the similarities between tidal and wind turbines, vane type VGs were selected for this project. The parameters examined during the wind tunnel investigation were the VG shape, height, h, angle, β, distance between VG pairs, D, number of VG rows and vane curvature. In the interest of brevity, only part of the complete study [29] is presented here and results for VG shape, height, h, angle, β will be discussed. Based on the literature, the VG aspect ratio, the distance between VGs and the VG chordwise location were constant at $L/h = 3$, $d = 3.5h$ and $x_{VG} = 0.3c$, respectively. All the cases in this work are given in Table 1 and a schematic is given in Fig. 2.

The VGs were 3D printed on plates with thickness $t = 0.5\,mm$ and chordwise length 30 mm. It should also be noted that the total height of the VG vane includes the height of the baseplate. The effect of the base plate without the VGs on the airfoil performance was examined independently and it was found that at $\alpha = 0°$ the plate on its own causes a drag increase $\Delta C_{d,plate,free} = 0.0018$ and $\Delta C_{d,plate,fixed} = 0.0007$, under free and fixed transition conditions respectively. These values not normalised and are in good agreement with previous works [12].

2.3. Boundary layer height estimation

The performance of VGs depends on their relative height with

Table 1
Vortex Generator configurations.

VG name	VG vane shape	VG angle, β	VG height, h/c	VG pair distance, D/h	VG distance, d/h	VG Aspect Ratio, L/h
1a	◿	**10°**	1.0%	7	3.5	3
1b	◿	**15°**	1.0%	7	3.5	3
1c	◿	**20°**	1.0%	7	3.5	3
1d	◿	15°	**1.5%**	7	3.5	3
1e	◿	15°	**0.7%**	7	3.5	3
1f	◿	15°	**0.5%**	7	3.5	3
2a	□	**10°**	1.0%	7	3.5	3
2b	□	**15°**	1.0%	7	3.5	3
2c	□	**20°**	1.0%	7	3.5	3

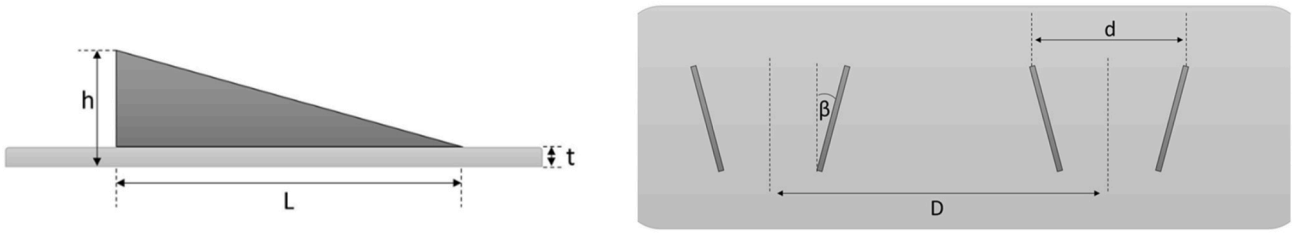

Fig. 2. Delta-shaped Vortex Generator parameters. (a) Side view; (b) Top view (flow coming from the bottom).

respect to the local boundary layer height [9]. The latter was estimated based on XFOIL [30] calculations. To simulate the wind tunnel free stream turbulence effect a parameter value of $n_{crit} = 5.5$ was used. XFOIL calculates the displacement thickness (δ^*), momentum thickness (θ) and transition locations. This information was used to calculate boundary layer heights before and after transition. Before the transition point, the laminar boundary layer height was calculated using Eq. (1) [31].

$$\delta = 2.9\delta^* \tag{1}$$

Downstream of the transition point, the turbulent boundary layer height was calculated using Eq. (2) [32].

$$\delta = \theta\left(3.15 + \left(\frac{1.72}{H-1}\right)\right) + \delta^* \tag{2}$$

The local boundary layer height at the location of the VGs at $\alpha = 6^\circ$ for all the flow conditions examined is given in Table 2. The specific AoA was selected as it is the design AoA for the profile under investigation under rated operational conditions.

2.4. Computational Fluid Dynamics approach

2.4.1. Solver

For the numerical part of the investigation, MaPFlow [33], an in-house unsteady Reynolds-Averaged Navier Stokes (URANS) solver with VG modelling capabilities [34–36] was used. MaPFlow is capable of solving both compressible and fully incompressible flows in arbitrary polyhedral meshes, using a cell-centred finite volume discretization process. In all cases presented here, the flow was treated as fully incompressible and for the turbulence closure, the two-equation model by Menter (k-ω SST) was used [37].

2.4.2. Vortex generator modelling

Regarding the vortex generator modelling the jBAY model [38] is employed following the guidelines presented in Ref. [34]. According to the model, a force source term is added to the momentum equations at the cells that engulf the VG [38]. The added force term is

$$\vec{L} = \sum \vec{L}_i \tag{3}$$

where $\vec{L}_i$ is the source term added to the momentum equations at the cells where the model is applied. $\vec{L}_i$ is given by Eq. (4)

$$\vec{L}_i = c_{VG} S_{VG} \frac{V_i}{\sum V_i} \rho |\vec{u}|^2 (\hat{u} \bullet \hat{n})(\hat{u} \times \hat{b})(\hat{u} \bullet \hat{t}) \tag{4}$$

Table 2
Boundary layer height (δ) at the location of the Vortex Generators based on XFOIL calculations at $\alpha = 6^\circ$.

Reynolds Number	Free transition			Fixed transition		
	0.65×10^6	1.0×10^6	1.5×10^6	0.65×10^6	1.0×10^6	1.5×10^6
δ/c	0.011	0.008	0.004	0.017	0.015	0.014

where c_{VG} is the BAY model constant, V_i is the grid cell volume and the unit vectors $\hat{n}, \hat{b}, \hat{t}$ are defined in Fig. 3, left. The constant c_{VG} is the only model parameter and acts as a relaxation parameter, controlling the strength of the force term. In this work the constant was defined as $c_{VG} = 10$. An example of VG cell selection is given schematically in Fig. 3, right.

2.4.3. Airfoil simulations set-up

For the airfoil simulations, which were used to benchmark our computational approach against the wind tunnel results, a single VG was simulated to reduce the required computational time. A two-dimensional numerical grid consisting of 114000 cells was extruded in the spanwise direction to create the limited aspect ratio computational domain ($z_{max} = D/2$) required for the simulations, see Fig. 3 right. The 2D grid was extruded in 22 equidistant cells, which corresponds to 6 cells in the span direction of the VG. For the interested reader, more details on the numerical set up including the grid dependence study is reported in Ref. [39].

2.4.4. Blade simulations set-up

Regarding the tidal turbine blade simulations, the computational domain is shown in Fig. 4, left. The domain extends 10 rotor diameters (D) in the radial direction and 30 D in the streamwise direction. Only one blade is considered with 120° periodic conditions. In addition to the rotor blade, the rotor hub and a cylindrical nacelle is also modelled, see Fig. 4, right. The nacelle is extended up to 0.85 blade radii to ensure that any separation at the end of the nacelle will not significantly affect the flow on the blade.

When it comes to chosing the mesh parameters, there are several requirements to fullfilled. Initially, for all the work presented here the maximum y + value is below 2. The boundary layer consisted of 30 layers with a growth rate of 1.2. Regarding the spanwise cell distribution and the wake refinement region, it was found that grids consisting of a total ~15 million cells with 30 thousand cells on the blade surface were sufficient to get grid independend results regading power and torque. However, this kind of meshes did not provide enough spatioal resolution for the modelling of VG's.

As detailed in section 2.4.2, the VG's are modelled using the BAY model approach. Employing the BAY model can significantly facilitate mesh generation, however, the grid used must be fine enough, otherwise the VG trailing vortex will be underestimated. As suggested in Ref. [34] at least 4 grid cells in the spanwise should be used to resolve the VG. Consequently, when considering large arrays consisting of several VG's the mesh requirements become much stricter.

To this end, the meshes we finally employed consist of approximately 40–50 million cells depending on the VG array deployed. The boundary layer parameters (y+ and number of layers) were the same for all meshes, however, the surface mesh was refined in the location of the VG array to ensure that each VG was resolved by at least 4 cells. This resulted in hybrid surface meshes consisting of 400–500 thousand cells. An example of the surface mesh on the blade is given in Fig. 5, where the VG cells are also highlighted.

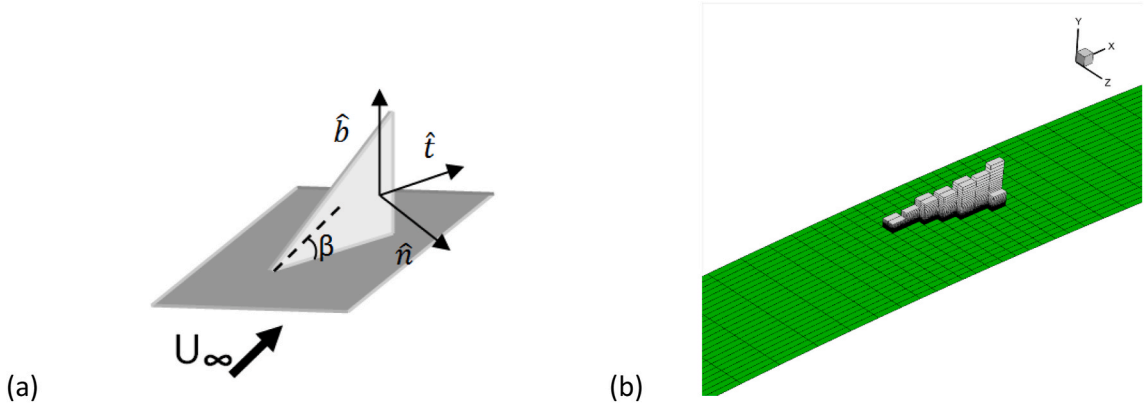

Fig. 3. (a) Unit vectors for a triangular VG geometry. (b) Detail of the airfoil surface computational grid (in green) also showing the cells where the jBAY model is applied (in grey).

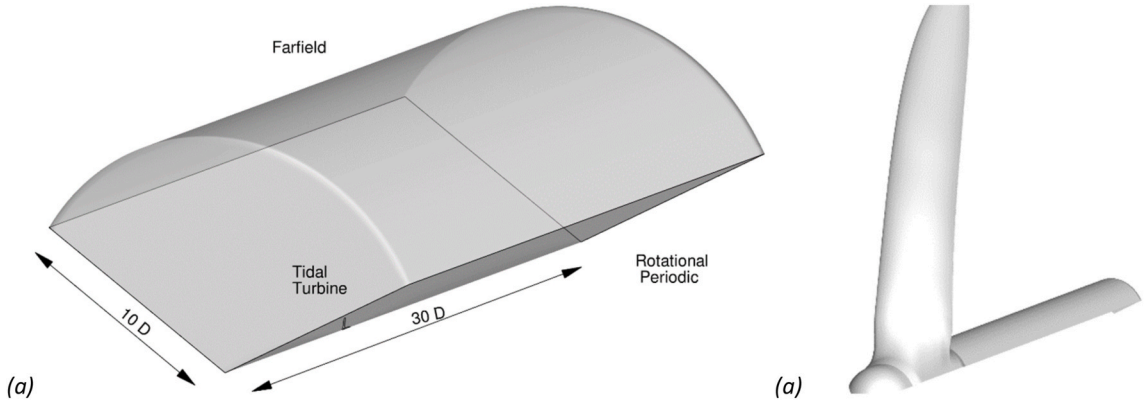

Fig. 4. (a) The computational domain used for the CFD simulations of the tidal turbine with the basic domain dimensions shown; the farfield extends 10 diameters in the radial direction and 30 diameters in the streamwise direction with periodic boundaries at the sides. (b) A closer view of the tidal turbine blade, nacelle and hub.

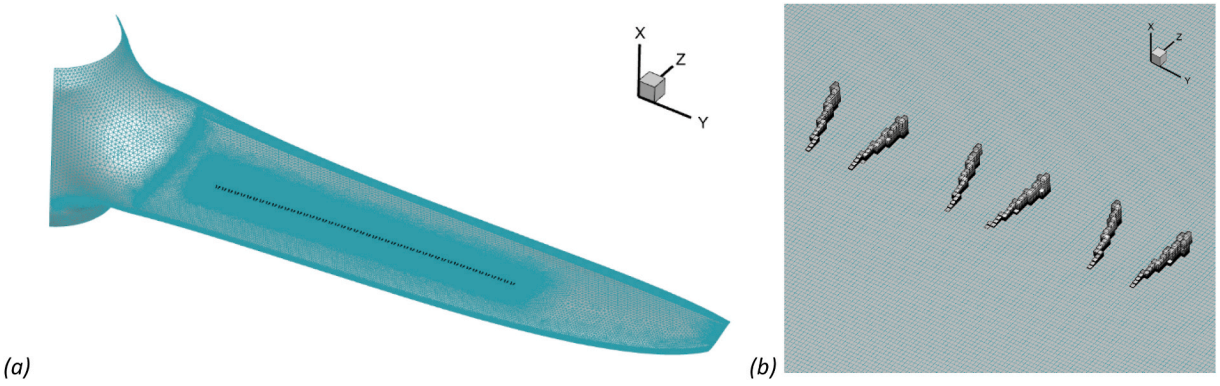

Fig. 5. (a) Surface mesh for the full-size blade resolved simulations with VGs. The cells where the BAY model was applied (VG cells) are also highlighted in black. (b) Detail of the VG cells on the blade surface.

3. Results and discussion

In this section all results are presented and discussed, starting with the wind tunnel data and followed by the CFD predictions. It is noted that, unless otherwise started, airfoil lift and drag coefficient values are normalised with the maximum lift and the minimum drag coefficient (Cd at $\alpha = 0^\circ$) for the baseline airfoil with fixed transition, respectively.

3.1. Baseline airfoil results

First, the results of the 0.2c thick airfoil without VGs are presented for free and fixed conditions at a Reynolds number of $Re = 10^6$. As illustrated in Fig. 6, the lift gradient in the linear region is the same for both free and fixed conditions. Under fixed conditions, lower lift coefficients are observed due to the decambering of the airfoil by the thicker, turbulent boundary layer, with a difference of $\Delta C_l = 0.031$ at 0°, in normalised values. Furthermore, stall occurred earlier as the ZZ tape extracted energy from the boundary layer causing flow separation

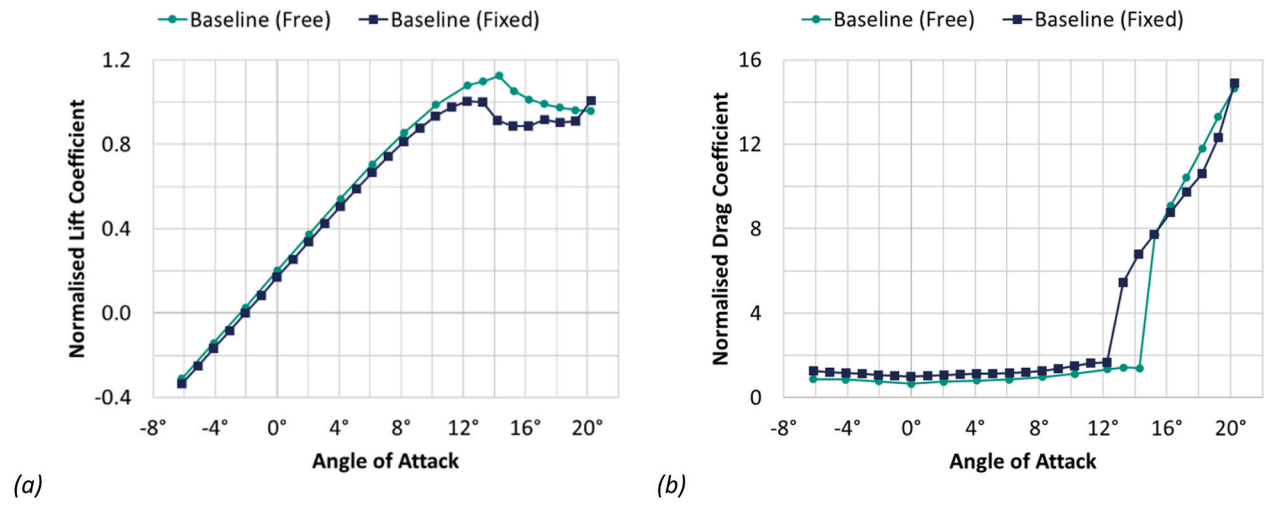

Fig. 6. Normalised lift (a) and drag (b) coefficient variation with angle of attack for the baseline airfoil under free and fixed transition conditions at a Reynolds number of $Re = 10^6$.

to occur at a lower AoA. Under free transition conditions, maximum lift was higher by 12.2% compared to fixed transition case. As expected in the linear region, the addition of ZZ tapes increased drag with an increase of $\Delta C_d = 0.346$ at $\alpha = 0°$, again in normalised values.

3.2. Vortex generator wind tunnel parametric study

The wind tunnel VG parametric study is presented in this section. The examined parameters are vane shape, angle and height and a suitable configuration for the airfoil profile under investigation is identified. The selected VG set up was subsequently tested under free transition and for the complete Re number range.

3.2.1. Vortex generator vane shape and angle

Two vane planforms were assessed, delta (or triangular) and rectangular-shaped, for all vane angles. The lift and drag coefficient polars are given in Fig. 7, Figs. 8 and 9 for $\beta = 10°, 15°$ and 20°, respectively. Main values are summarised in Table 3.

At the lowest vane angle, $\beta = 10°$, both VG types led to similar drag increase. For higher vane angles, however, it was found the rectangular shaped vanes produced more drag, in agreement with existing literature [9,11]. Triangular VGs produced the same drag for $\beta = 10°$ and $\beta = 15°$ with an increase for $\beta = 20°$. In terms of flow separation control, all configurations extended the linear part of the lift curve by 4° (from $\alpha = 6°$ to $\alpha = 10°$). The highest lift values before stall were observed for the triangular VGs at $\beta = 15°$ and the highest $\alpha_{C_{l,max}}$ was observed for triangular VGs at $\beta = 10°$. In the remaining of this document only delta shaped VGs will be considered.

3.2.2. Vortex generator vane height

The effect of vane height was assessed on delta shaped VGs with a vane angle of $\beta = 15°$, which produced the maximum lift to drag ratio. Force coefficient and lift to drag ratio polars are presented in Figs. 10 and 11, respectively.

In terms of lift to drag ratio, the smaller vane heights are superior to larger VGs, as illustrated in Fig. 10 (a). The best performing configuration in terms of maximum lift to drag ratio was the 0.7%c VG type (VG1e), see Table 4.

In the linear region, low profile VG configurations (VG1e and VG1f) produced less drag with an increase of approximately 14.5% at $\alpha = 0°$. On the other hand, an increase of approximately 26% was observed for higher VGs (VG1d and VG1b), see Table 4. Low profile VG configurations also delay flow separation for longer than higher vane heights, as illustrated in Fig. 10 (a). Decreasing the vane height to $h_{VG} = 0.5\%c$, led to a loss in effectiveness in delaying flow separation compared to $h_{VG} =$

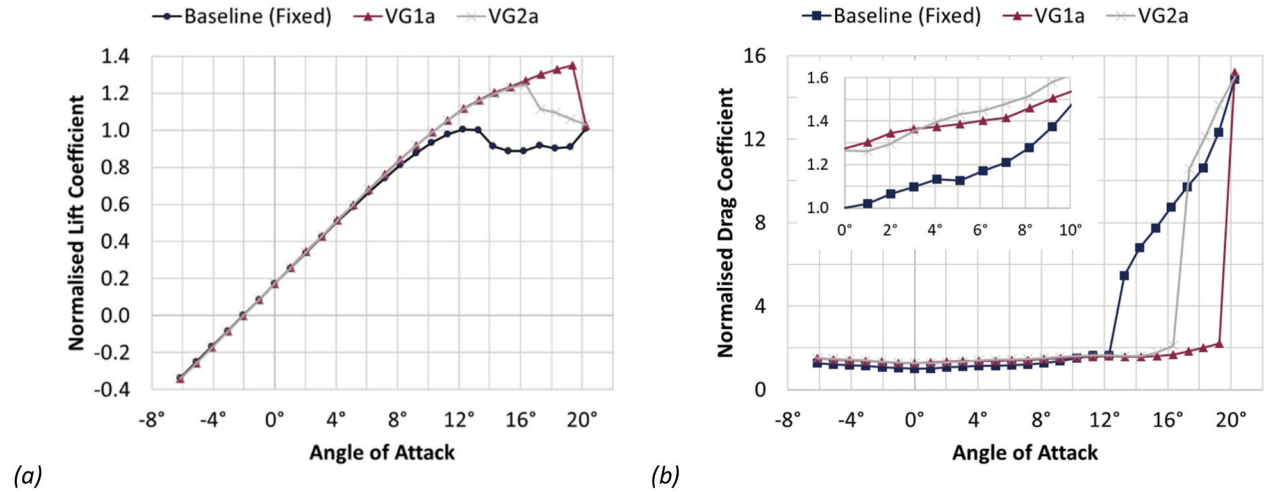

Fig. 7. Normalised lift (a) and drag (b) coefficient variation with angle of attack comparing delta and rectangular shaped vane with a vane angle of $\beta = 10°$ testing at a Reynolds number of $Re = 10^6$ under fixed transition conditions.

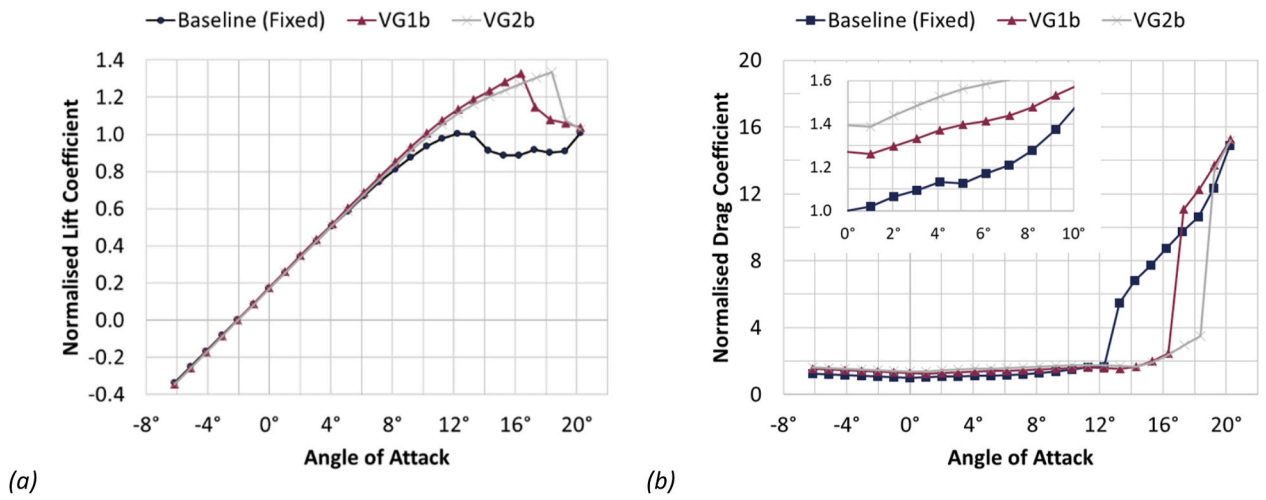

Fig. 8. Normalised lift (a) and drag (b) coefficient variation with angle of attack comparing delta and rectangular shaped vane with a vane angle of $\beta = 15^{\circ}$ testing at a Reynolds number of $Re = 10^6$ under fixed transition conditions.

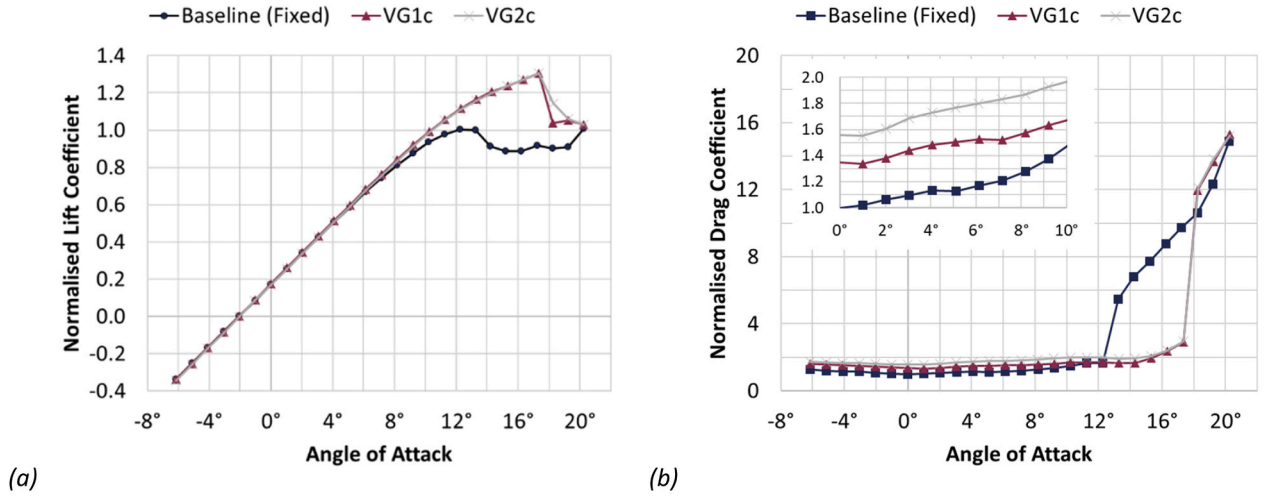

Fig. 9. Normalised lift (a) and drag (b) coefficient variation with angle of attack comparing delta and rectangular shaped vane with a vane angle of $\beta = 20^{\circ}$ testing at a Reynolds number of $Re = 10^6$ under fixed transition conditions.

Table 3
Vortex Generator shape and angle effect on force coefficients compared to the fixed transition baseline. Fixed transition conditions, $Re = 10^6$.

	Delta-shaped VGs			Rectangular-shaped VGs		
VG name	VG1a	VG1b	VG1c	VG2a	VG2b	VG2c
Vane Angle, β	10°	15°	20°	10°	15°	20°
$\Delta C_{d,\alpha=0^{\circ}}$	27.5%	27.3%	34.5%	26.4%	39.3%	55.7%
$\Delta C_{l,max}$	35.0%	32.8%	30.0%	24.7%	33.5%	30.4%
$\Delta L/D_{max}$	20.2%	20.6%	13.1%	17.2%	11.9%	2.9%

0.7%*c* as well as poorer lift characteristics in the linear region. It is noted that this VG height ($h_{VG} = 0.7\%c$) is equal to $h_{VG} = 0.5\delta$ for the fixed transition case presented in Fig. 10 ($Re = 1M$, see also Table 2). The present results show that VGs with a height lower than the local boundary layer (AKA low-profile VGs) perform better than larger VGs, in agreement with [9].

3.2.3. Selected vortex generator configuration

The best performing VG configuration in terms of maximum lift to drag ratio increase, VG1e, was chosen for further assessment under free transition conditions and in the Re number range from $0.65x10^6$ to $1.5x10^6$. The main geometrical parameters are summarised in Table 5.

The performance of the profile with VGs under both free and fixed transition cases is shown in Fig. 12. In free transition with VGs, stall is delayed beyond $\alpha = 20^{\circ}$. Due to the increased drag, L/D drops at low AoA, but is increased for $\alpha > 12^{\circ}$ compared to the uncontrolled case.

In the fixed transition case, the addition of VGs delays the onset of stall throughout the range of Re numbers assessed in this study, as illustrated in Fig. 13 (a). In terms of maximum lift to drag values, the VGs increase performance for all Reynolds numbers, see Fig. 13 (b). It is seen that the lift to drag ratios are reduced with the linear region but are increased significantly at higher AoA where the flow separation is controlled. The effect decreases with decreasing Re number, as the relative VG height with respect to the boundary layer height also decreases.

3.3. CFD numerical investigation

In this section the results from the CFD investigation are presented. First, the VG modelling capabilities are confirmed for the airfoil case by comparing the numerical predictions to the wind tunnel measurements. Subsequently, the full blade geometry is resolved and the flow is simulated with and without VGs in model scale and in full-size.

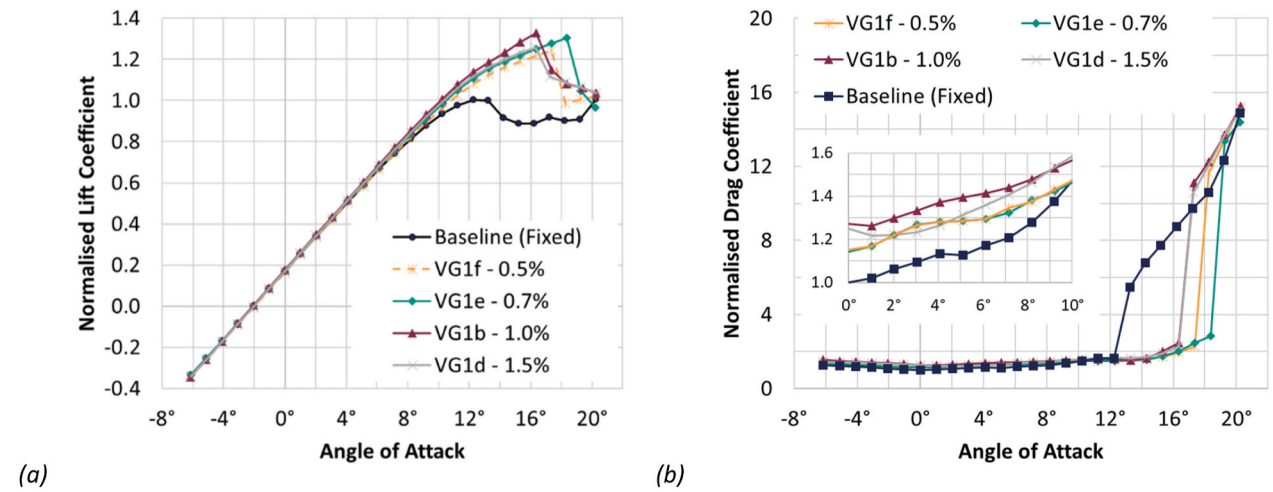

Fig. 10. Normalised lift (a) and drag coefficient (b) variation with angle of attack for varying vortex generator vane heights while testing at Reynolds number of $Re = 10^6$ under fixed transition conditions.

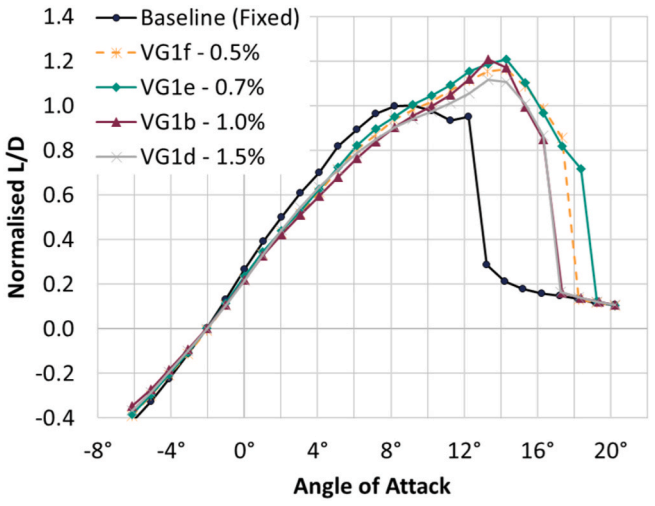

Fig. 11. Normalised lift to drag ratio variation with angle of attack for varying vortex generator vane heights while testing at a Reynolds number of $Re = 10^6$ under fixed transition conditions.

Table 4
Vortex Generator height effect on force coefficients compared to the fixed transition baseline. Delta shaped Vortex Generators with $\beta = 10°$. Fixed transition conditions, $Re = 10^6$.

VG name	VG1f	VG1e	VG1b	VG1d
Vane height, h/c	0.5%	0.7%	1.0%	1.5%
$\Delta C_{d,\alpha=0°}$	15.2%	14.3%	27.3%	25.1%
$\Delta C_{l,max}$	24.3%	30.6%	32.8%	25.6%
$\Delta(L/D)_{max}$	20.7%	20.8%	16.6%	11.6%

Table 5
Selected Vortex Generator configuration parameters.

Selected VG	VG angle, β	VG height, h/c	VG pair distance, D/h	VG distance, d/h	VG Aspect Ratio, L/h
VG1e	15°	0.007	7	3.5	3

3.3.1. Vortex generators on the tidal turbine profile

The CFD predictions for the VG effect on the airfoil force coefficients and the relative experimental results are given in Fig. 14. The comparison in terms of pressure distribution along the profile chord is presented in Fig. 15. The relative effect is captured very well in the numerical predictions, especially in the linear lift region. The drag penalty due to the application of VGs is also predicted well. Disagreement at higher AoA is expected due to the presence of three-dimensional coherent structures of separated flow known as stall cells [40,41]. Two-dimensional and low aspect ratio simulations, like the ones used in this study are not capable of capturing the phenomenon [35,36]. This also explains the disagreement in pressure coefficient distribution at $\alpha = 15°$, Fig. 16 (a), where the separated flow pressure plateau is more extended in the experiments than in the simulations. Overall, the VG modelling approach is considered acceptable. Consequently, the same method is employed for the blade resolved simulations presented in the following section.

3.3.2. Vortex generators on the model scale tidal turbine blade

For the application of the VGs on a tidal turbine blade, the model scale test case presented in Ref. [26] is considered first. In that study, a 1:8 scaled (maximum radius $R = 0.25\ m$) brass model of the SCHOTTEL SIT250 tidal turbine was tested without VGs. The previously published experiments are used as a validation case for the blade resolved CFD approach and then the effect of applying VGs on the specific turbine is predicted using RANS CFD simulations. The comparison between measurements and numerical predictions for the thrust and power coefficient is given in Fig. 17. The agreement between the experiments and simulations is considered good, especially for $2 \leq \lambda \leq 8$.

The case with the VGs was only examined numerically as no relevant experimental data are available. The chordwise skin friction contours and skin friction lines on the blade suction side with and without vortex generators are presented in Figs. 18 and 19, for $\lambda = 4$ and 5, respectively. It is noted that the region of separated flow on the blade suction side is extremely limited at higher λ values, while for $\lambda < 4$, the flow separation line is close to the blade leading edge, well upstream of the VGs. Hence, the VGs are expected to affect the flow mostly for the specific tip speed ratio values ($\lambda = 4$ and 5).

The VG placement was based on the CFD results of the baseline case. The VGs were located just upstream of the separation line to minimise drag penalty without limiting their effectiveness. It is noted that a single VG placement was considered, since this is a proof-of-concept investigation and not an optimization study.

Starting with the baseline uncontrolled case (top part of Figs. 18 and

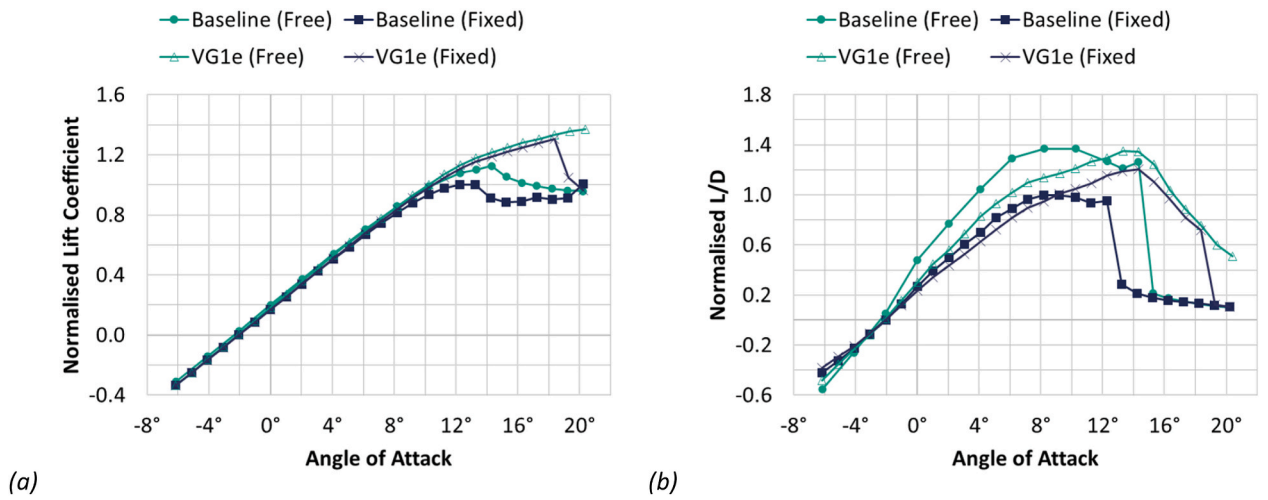

Fig. 12. Normalised lift coefficient (a) and lift to drag ratio (b) variation with angle of attack for VG1e compared to the baseline while testing at Reynolds number of $Re = 10^6$ under free and fixed transition conditions.

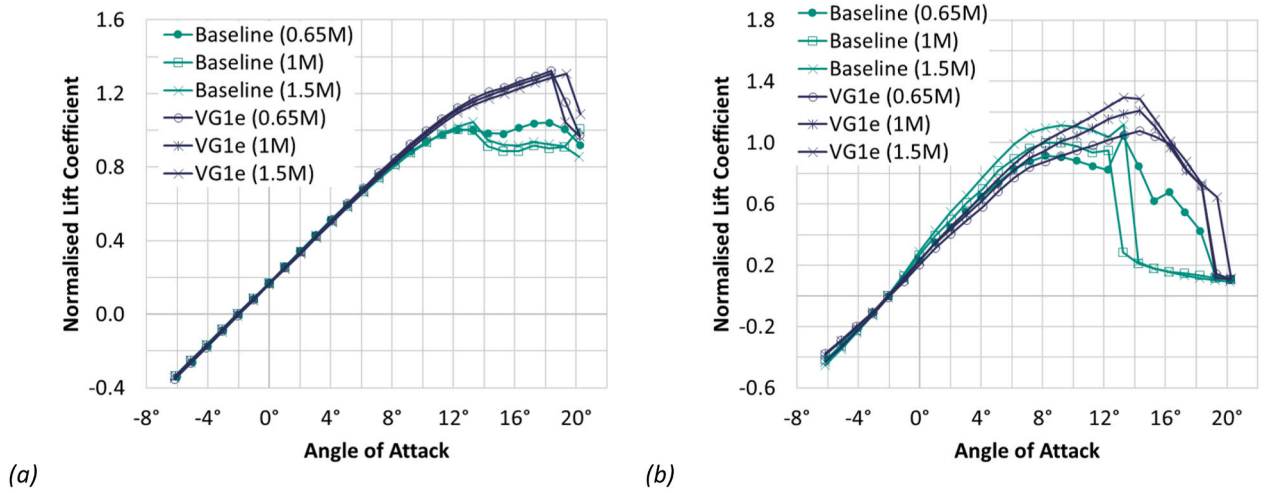

Fig. 13. Normalised lift coefficient (a) and normalised lift to drag ratio (b) variation with angle of attack for VG1e compared to the baseline for different Reynolds numbers under fixed transition conditions.

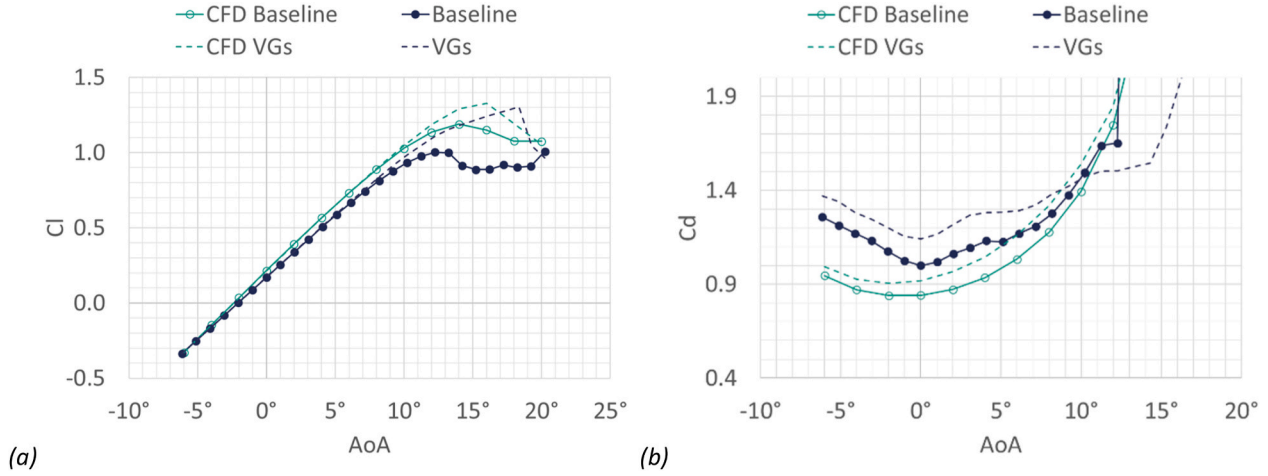

Fig. 14. Normalised lift (a) and drag (b) coefficient variation with angle of attack with and without the selected VG configuration (VG1e). Comparison between fixed transition wind tunnel experiments and CFD results at $Re = 10^6$.

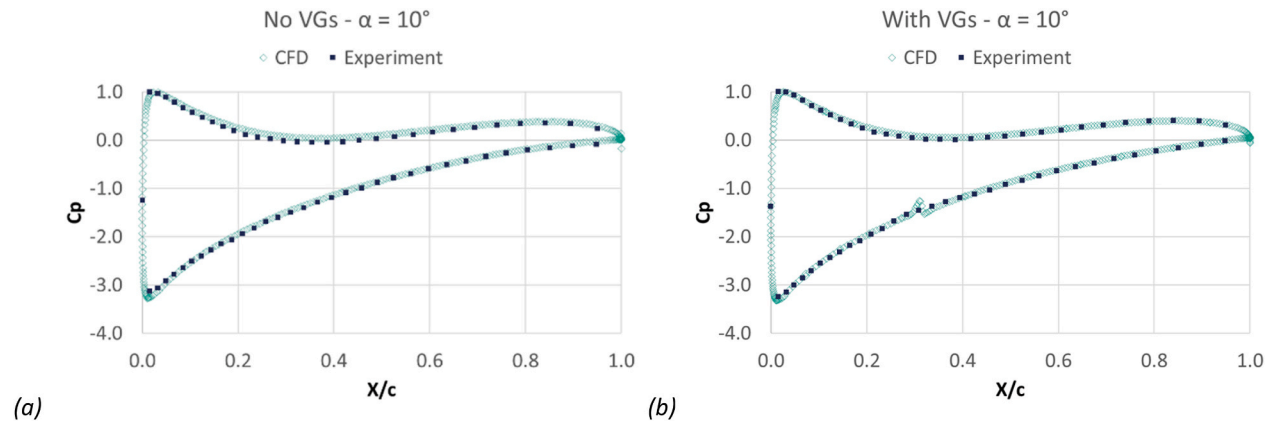

Fig. 15. Pressure coefficient distribution along the profile chord with and without Vortex Generators at $\alpha = 10°$. Comparison between fixed transition wind tunnel experiments and CFD results at $Re = 10^6$.

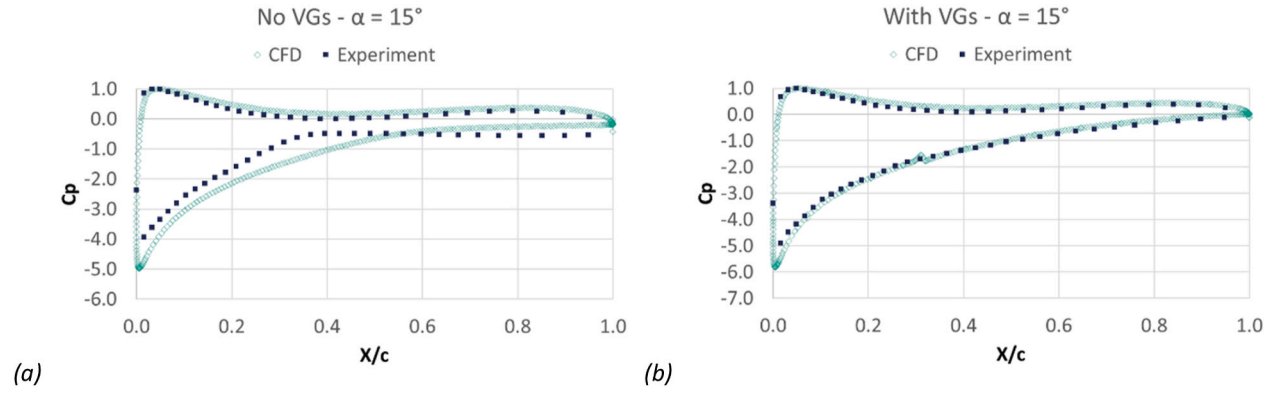

Fig. 16. Pressure coefficient distribution along the profile chord with and without Vortex Generators at $\alpha = 15°$. Comparison between fixed transition wind tunnel experiments and CFD results at $Re = 10^6$.

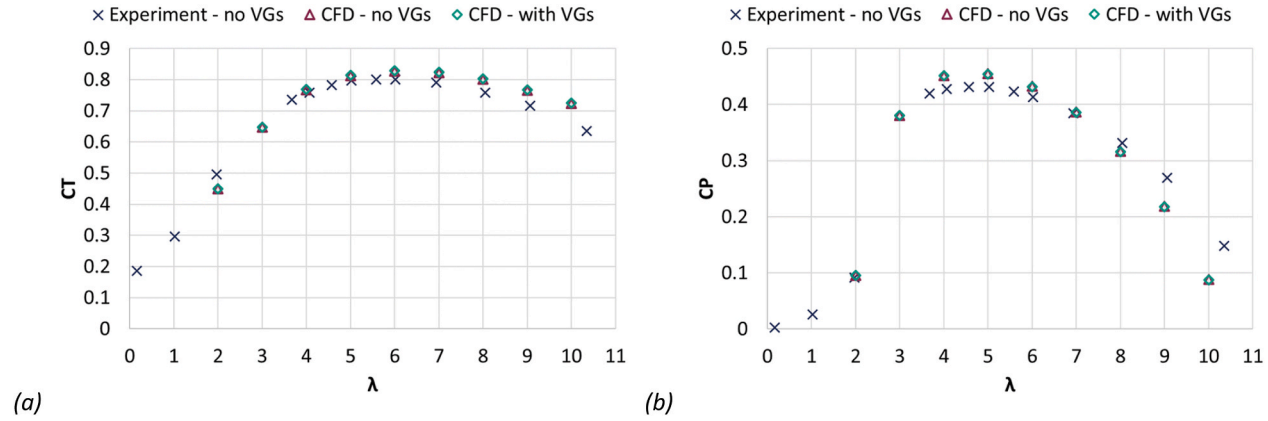

Fig. 17. (a) Thrust and (b) power coefficient variation with tip speed ratio. Comparison between towing tank experiments and CFD results for an inflow velocity of $V_\infty = 2.0\,m/s$.

19), three-dimensional separation is observed in the root region, up to $y = 40\%\,R$ and $y = 28\%\,R$ for $\lambda = 4$ and 5, respectively. Significant radial flow is observed inside the separated flow region close to the root, while upstream of the separated flow substantial radial flow is also noted.

The effect of the VGs on the flow is illustrated by the changes in the skin friction contours and in the surface flow lines (see lower part of Figs. 18 and 19). Separation is significantly reduced for both $\lambda = 4$ and 5, down to $y = 29\%\,R$ and $y = 24\%\,R$, respectively. The extent of radial flow is also significantly reduced downstream of the VGs.

The VG effect on performance and loads is less pronounced, as illustrated by the thrust and power coefficient curves in Fig. 17. This is in agreement with Blade Element Momentum (BEM) predictions for the same blade [25], where a performance improvement of 0.5% at $\lambda = 5$ was predicted. Further examination suggests that indeed the normal and, most importantly, the tangential force on the blade is not significantly affected by the presence of the VGs, see Fig. 20.

The reason behind this is shown in Fig. 21, where the pressure

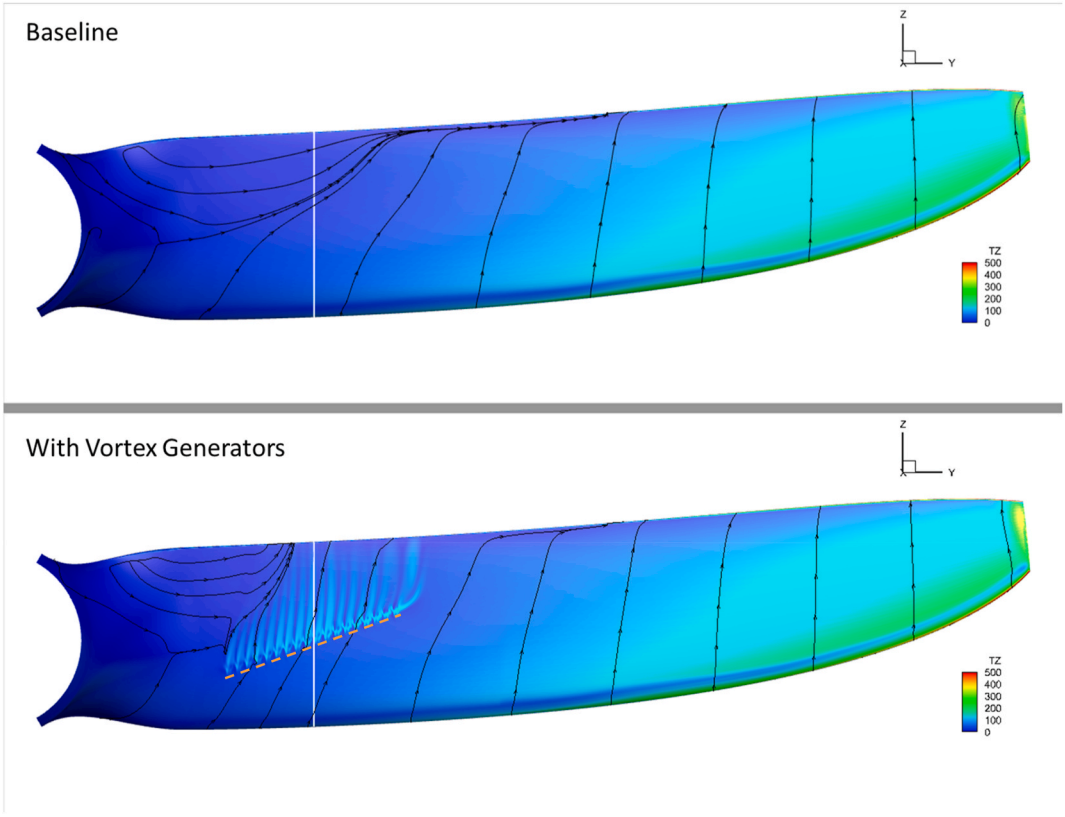

Fig. 18. Chordwise skin friction (TZ) contour on the blade suction side without (top) and with vortex generators (bottom) for $\lambda = 4$ and an inflow velocity of $V_\infty = 2.0\, m/s$. TZ units are N/m^2. The white vertical line and the dashed orange line indicate the $y = 0.31R$ and the Vortex Generators' location, respectively.

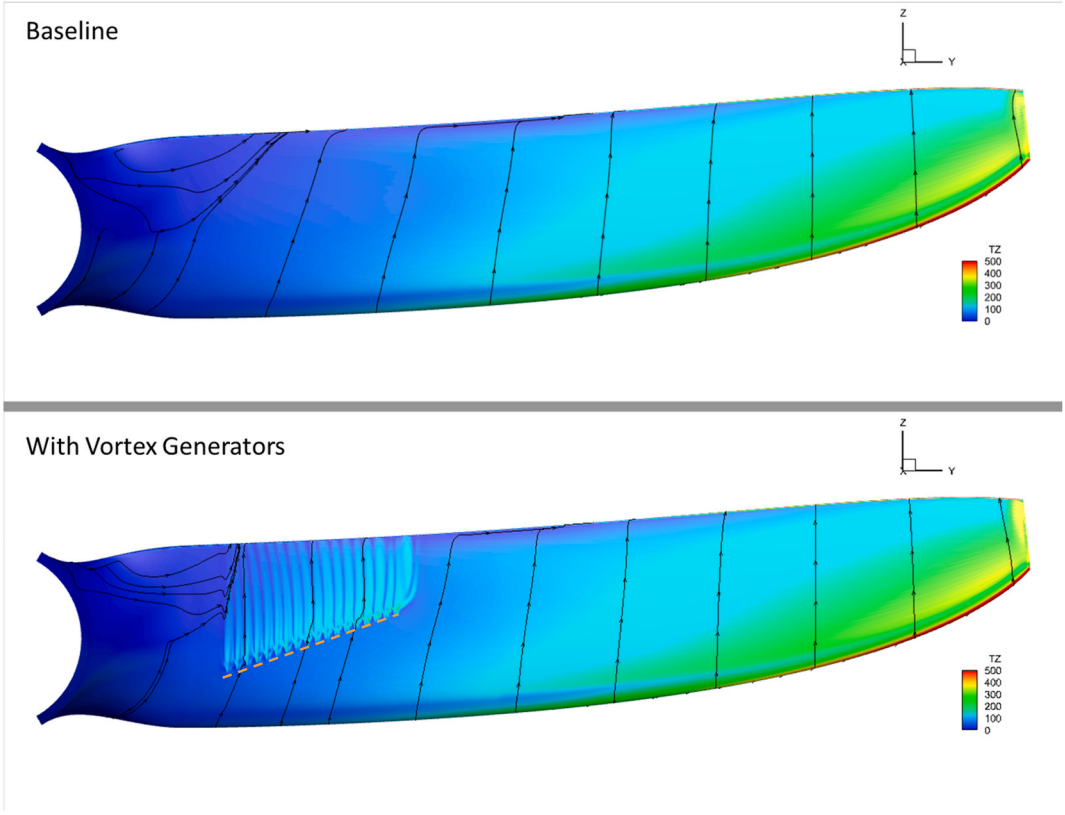

Fig. 19. Chordwise skin friction (TZ) contour on the blade suction side without (top) and with vortex generators (bottom) for $\lambda = 5$ and an inflow velocity of $V_\infty = 2.0\, m/s$. TZ units are N/m^2. The dashed orange line indicates the Vortex Generators' location.

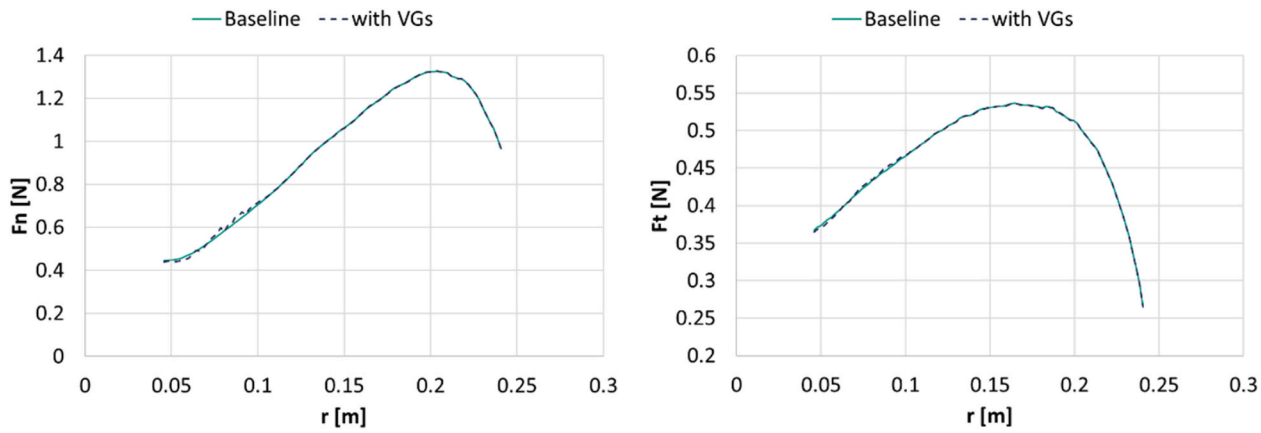

Fig. 20. Normal and tangential forces on the turbine blade with and without vortex generators for $\lambda = 4$ and an inflow velocity of $V_\infty = 2.0\,m/s$.

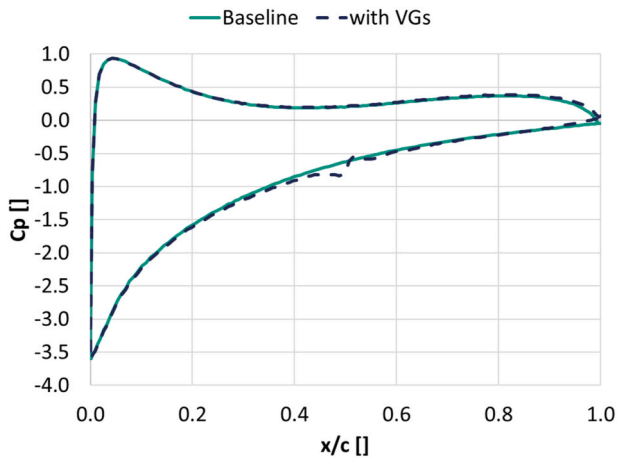

Fig. 21. Pressure coefficient distribution along the blade chord at $y = 0.31R$ for $\lambda = 4$ and an inflow velocity of $V_\infty = 2.0\,m/s$.

coefficient distribution along the blade chord at $z = 0.31R$ is plotted. The specific spanwise location is highlighted in Fig. 18 for clarity and was selected to investigate the effect of the VGs on the pressure close to the root region where they successfully suppress separation. What is observed is that the pressure distribution with or without the VGs changes very slightly. This contrasts with the non-rotating profile results, see Fig. 16, where the presence of the VGs eliminates the pressure plateau caused by the separated flow close to the trailing edge.

In the case of the rotating blade, despite the presence of the separated flow region, no such plateau is observed. This is attributed to the effect of rotation on the flow. As detailed in Ref. [42], the centrifugal loads on the separated volume of fluid near the trailing edge lead to radial flow, see also Figs. 18 and 19, top. In the rotating case, the reversed flow region is reduced and the radial flow leads to a stronger pressure recovery towards the trailing edge [43]. As a result, the elimination of separated flow from the blade root region by the VGs does not result in a significant pressure distribution change (see Fig. 21) because the separated flow does not correspond to a pressure plateau as in the 2D Wind Tunnel experiments. This is due to the significance of rotational augmentation for the scale model tidal turbine [42,43]. In fact, the rotational effect in this case is so significant that there is a considerable component of radial flow even for the attached flow upstream of the VGs and rotational effects are more pronounced closer to the root than the tip, in agreement with [43].

It is noted at this point that rotational effects are stronger for higher rotational speed and lower Reynolds numbers [43]. In the scaled turbine case examined here, the Reynolds number is low (at the order of 250k) and the rotational speed high ($\omega \approx 32\,rad/s$ for $l = 4$). To put this into context, the full-size 85 kW tidal turbine would rotate at $\omega = 4\,rad/s$ for the same inflow ($V_\infty = 2\,m/s$) and tip speed ratio. The relative values for a 10 MW wind turbine, where VGs have proven efficient [44], are given in Table 6, where the orders of magnitude difference can be observed. This indicates that the model scale turbine is not a suitable platform for the positioning of VGs mainly because the flow at low tip speed ratio is dominated by rotational effects.

3.3.3. *Vortex generators on the full-size tidal turbine blade*

The flow over the full-size turbine blade was simulated to examine the effect and suitability of VG flow control under realistic Reynolds number and rotational speeds. The blade geometry was scaled up to $R = 2.0\,m$, while the inflow velocity was the same as for the model scale, $V_\infty = 2.0$ m/s, which is a realistic inflow velocity for a tidal turbine site [45].

Fig. 22 shows the thrust and power coefficient variation with tip speed ratio for the model-size and full-size blades. The surface streamlines on the full-size blade suction side without VGs for $\lambda = 3$ and $\lambda = 4$ is shown in Figs. 23 and 24, respectively. The performance of the full-size case is significantly better, especially at high tip speed ratios, as it performs at much higher Reynolds numbers [46]. The low λ range, however, is of greater interest for the application of VGs, as this is where the flow separates. Contrary to the model scale blade, where the flow is fully separated for $\lambda = 3$ and partially separated for $\lambda = 4$ (Fig. 18, top), the full-size blade experiences extensive three-dimensional separated flow for $\lambda = 3$ (Fig. 23, top) and no separation for $\lambda = 4$ (Fig. 24, top). The dissimilarities are attributed to the Reynolds number difference and are key for locating the VGs on the blade.

In the present case, the VG location for the full-size blade was decided based on the streamlines for $\lambda = 3$ and is shown in Fig. 23, bottom. It is highlighted at this point that finding an optimal VG placement is out of the scope of this study. The effect of VGs on the surface streamlines for $\lambda = 3$ and $\lambda = 4$ is shown in Figs. 23 and 24, respectively. For $\lambda = 3$, the area of three-dimensional separated flow is significantly reduced, but not suppressed entirely. For $\lambda = 4$, the attached flow downstream of the VGs appears to be curved more

Table 6
Indicative operational conditions for different turbine scales.

	R [m]	V_∞ [m/s]	Typical ω [rad/s]	Indicative Re number
Scaled Tidal Rotor [26]	0.25	2	32.000	2.7E+05
Full-size 85 kW Tidal Rotor	2.00	2	4.000	2.1E+06
10 MW Wind Turbine [44]	89.17	10	0.841	1.2E+07

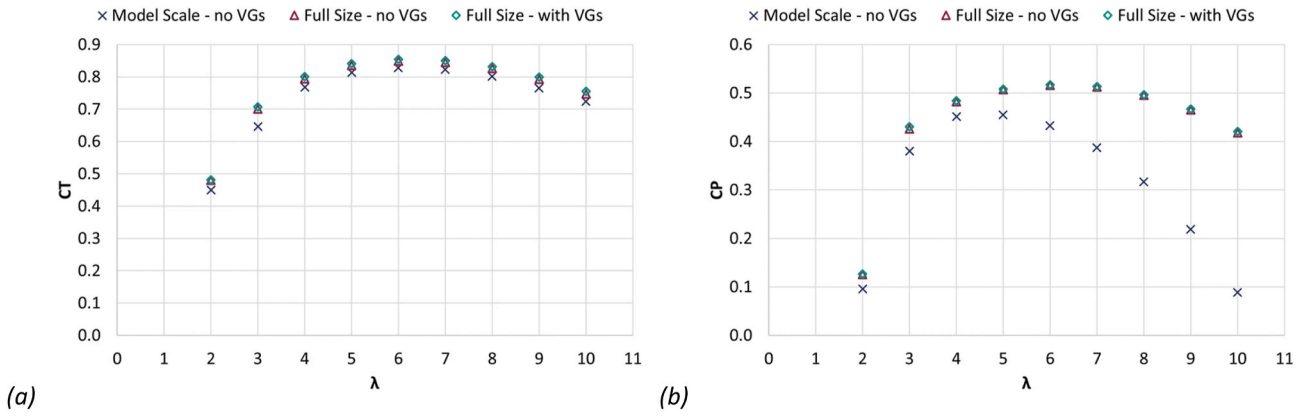

Fig. 22. (a) Thrust and (b) power coefficient variation with tip speed ratio. Comparison between model scale and full-size blade with and without Vortex Generators. CFD results for an inflow velocity of $V_\infty = 2.0\,m/s$.

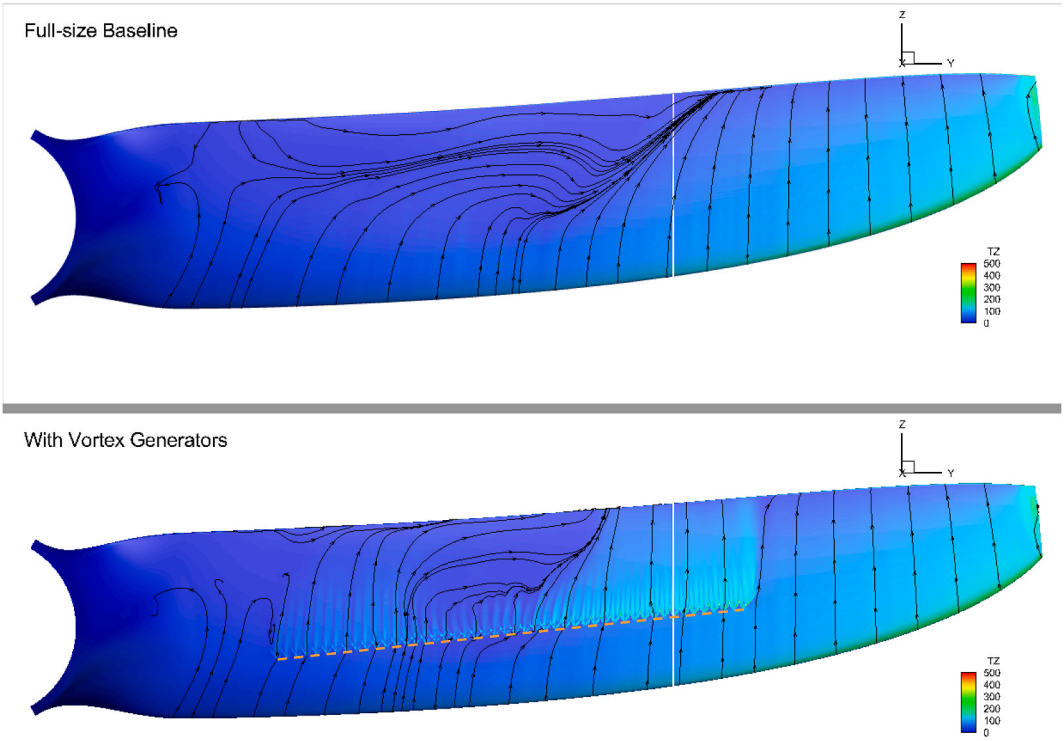

Fig. 23. Chordwise skin friction (TZ) contour on the full-size blade suction side without (top) and with vortex generators (bottom) for $\lambda = 3$ and an inflow velocity of $V_\infty = 2.0\,m/s$. TZ units are N/m^2. The solid white and the dashed orange line indicate the $y = 0.65R$ and the Vortex Generators' location, respectively.

towards the blade root than in the uncontrolled case. This is because the flow is accelerated by the presence of the VGs and as a result the Coriolis force, which points towards the blade root, is increased.

The performance of the full-size blade with VGs is also shown on Fig. 22 and the effect is positive for all tip speed ratios considered. The relative increase in power coefficient due to the presence of the VGs is presented in Fig. 25 with a maximum of 1.05% benefit for $\lambda = 3$. The effect of the VGs on the pressure variation along the blade chord at the radial station y = 0.65R for the same tip speed ratio is shown in Fig. 26. The VGs accelerate the flow over the suction side and eliminate flow separation at the specific station.

The effect of VGs on the normal and tangential loads on the full-size blade is given in Fig. 27. The beneficial effect on the tangential force is clear. At the same time, the maximum normal load is not increased by the presence of VGs. This is in agreement with the experience from the application of VGs on Wind Turbines where the retrofit addition of VGs does not require a new load specification for the wind turbine [47]. Finally, although this cannot be confirmed by the present simulations, it is expected that the reduction of the separated flow area will lead to a reduction on the unsteady loads on the blade.

4. Conclusions

The present study investigated the use of VGs as a passive flow control device on tidal turbine blades for the first time. Inspired by their application on horizontal axis wind turbines, the aim was to examine their effectiveness in suppressing the separated flow on the blade and thereafter improving performance.

To select a suitable VG configuration, a wind tunnel parametric study was performed for a 20% thick profile from Schottel's SIT250 tidal turbine. The wind tunnel experiments along with previously published model scale tidal turbine towing tank tests were further used to validate

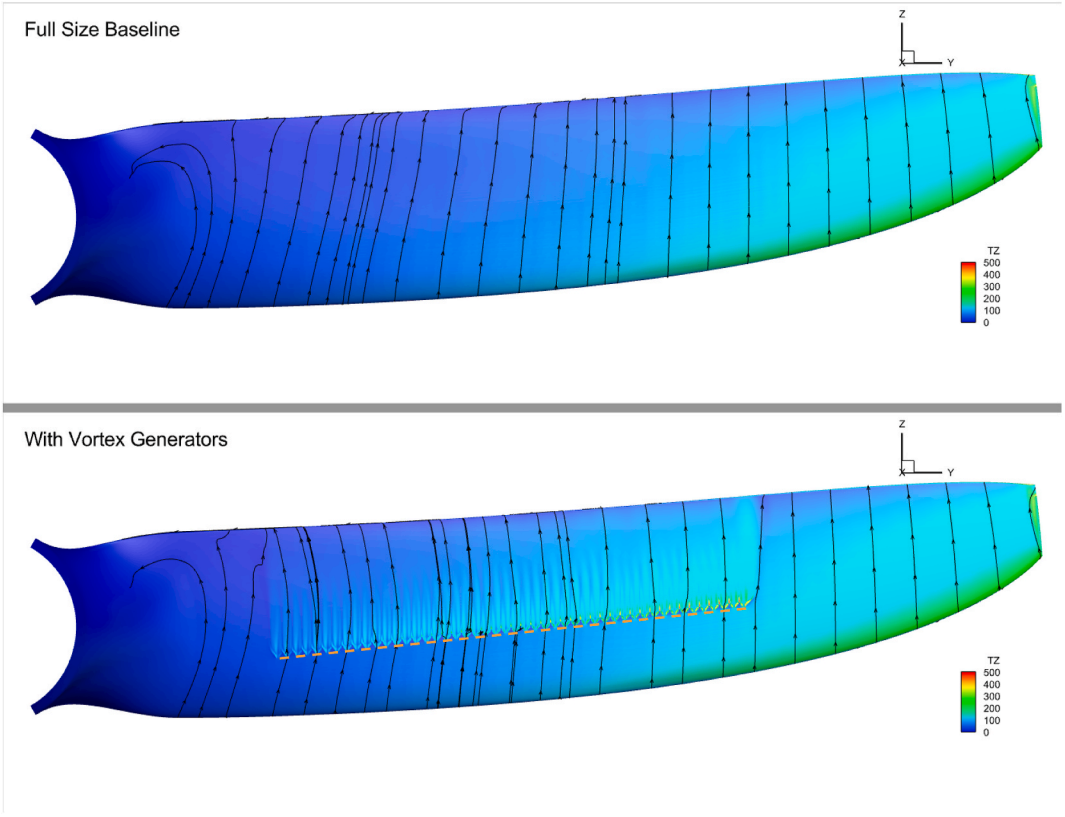

Fig. 24. Chordwise skin friction (TZ) contour on the full-size blade suction side without (top) and with vortex generators (bottom) for $\lambda = 4$ and an inflow velocity of $V_\infty = 2.0\,m/s$. TZ units are N/m^2. The orange dashed line indicates the location of the Vortex generators.

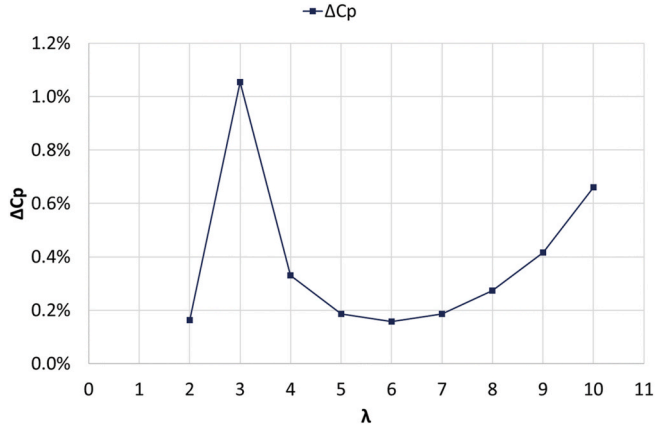

Fig. 25. Increase in power coefficient (C_p) due to the presence of Vortex Generators on the full-size blade for different tip speed ratios.

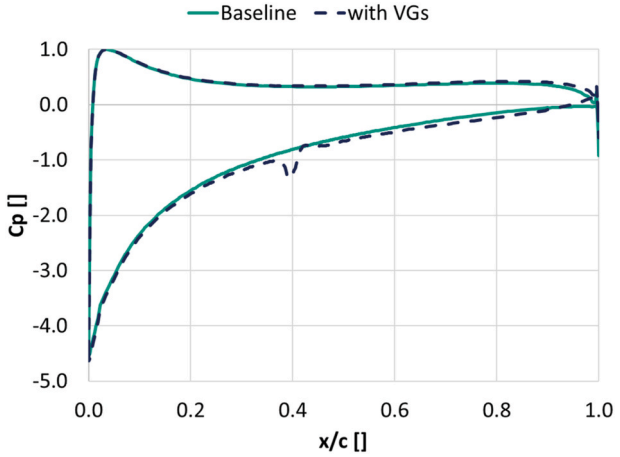

Fig. 26. Pressure coefficient distribution along the full-size blade chord at $y = 0.65R$ for $\lambda = 3$ and an inflow velocity of $V_\infty = 2.0\,m/s$.

a RANS CFD VG modelling approach. The agreement between the computational predictions and both experimental data sets was very good. The flow over the turbine blade was analysed under both model-scale and full-size operating conditions and the effect of VGs on both cases was investigated. It is noted that the VG placement on the blade was not optimized, as this was out of the scope of this study.

The main findings of the investigation are summarised below.

- Vane VGs on a typical tidal turbine blade profile behave as they would on a typical wind turbine profile blade, with sizing and locating parameters between the present study and the wind turbine relevant literature being very similar.
- The best performing vane VG configuration had a height of $0.007c$, which corresponded to a half the local boundary layer height (0.5δ) for operational Reynolds numbers.
- The model scale blade and the full-size blade have significantly different performance and flow patterns due to the large difference in Reynolds numbers and rotational speeds.
- The model scale blade experiences three-dimensional flow separation for $l = 4$ and $l = 5$. The full-size blade experiences extensive separation for $l = 3$.
- Vortex Generators successfully limit or even completely suppress flow separation on both the model scale and the full-size blade.

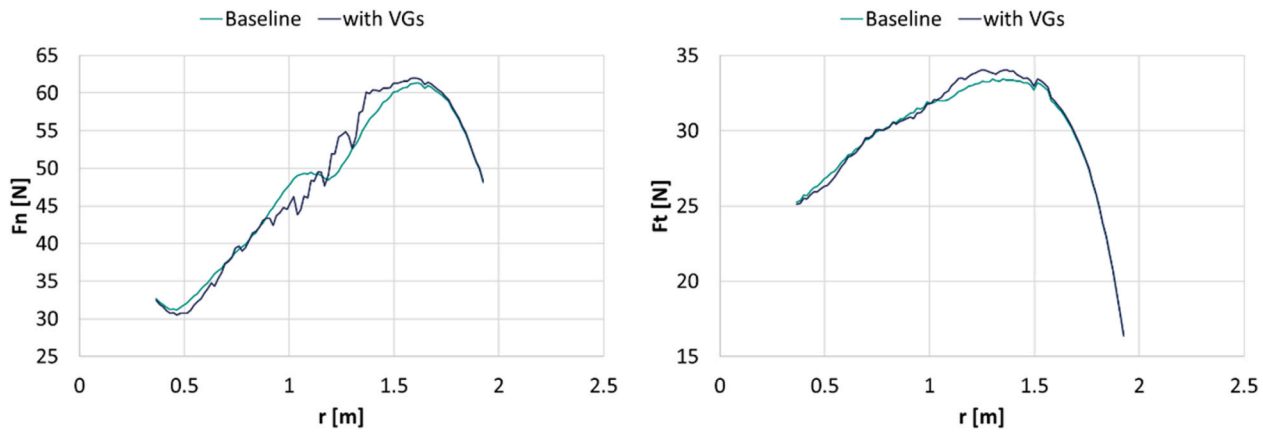

Fig. 27. Normal and tangential forces on the full-size turbine blade with and without vortex generators for $\lambda = 3$ and an inflow velocity of $V_\infty = 2.0\, m/s$.

- The rotational effect is very significant for the model scale blade, where low Reynolds numbers and high rotational speeds are combined.
- Due to the significant radial flow on the model scale blade, there is no pressure plateau where the flow is separated. As a result, the effect of suppressing separation by means of VGs on loads and performance is limited.
- The effect of VGs on the full-size blade is more pronounced and a maximum power coefficient improvement of 1.05% is predicted at $l = 3$.

The potential of the VGs to be included either in the design process of a tidal turbine blade or as a retrofit has been successfully illustrated. It is noted however, that the VG placement on the blade was not optimized and that greater gains would be possible if it was. Further, based on the present findings it is anticipated that VGs would perform even better for larger slower rotting blades. Finally, the reduction of separate flow on the blade is expected to reduce the unsteady loads on the blade, although this cannot be confirmed by the presently available data.

Funding

This research was funded by the EPSRC Impact Acceleration Account 2020 Research Impact Fund. Computational resources were provided by Supercomputing Wales, which is gratefully acknowledged.

CRediT authorship contribution statement

M. Manolesos: Conceptualization, Formal analysis, Data curation, Writing – original draft, Writing – review & editing, Visualization, Supervision, Project administration, Funding acquisition. **L. Chng:** Validation, Formal analysis, Investigation, Data curation, Writing – review & editing, Visualization. **N. Kaufmann:** Writing – review & editing, Funding acquisition. **P. Ouro:** Writing – review & editing, Funding acquisition. **D. Ntouras:** Software. **G. Papadakis:** Methodology, Software, Data curation, Supervision.

Declaration of competing interest

The authors declare that they have no known competing financial interests or personal relationships that could have appeared to influence the work reported in this paper.

References

[1] W.J. McCurdy, Investigation of Boundary Layer Control of an NACA 16-325 Airfoil by Means of Vortex Generators, United Aircr Corp, Res Dep Rept, 1948. M-15038-3.
[2] D.M. Rao, T.T. Kariya, Boundary-layer Submerged Vortex Generators for Separation Control - an Exploratory Study. 1st Natl. Fluid Dyn. Congr, AIAA, 1988, pp. 839–846.
[3] W.R. Pauley, J.K. Eaton, Experimental study of the development of longitudinal vortex pairs embedded in a turbulent boundary layer, AIAA J. 26 (1988) 816–823, https://doi.org/10.2514/3.9974.
[4] J.C. Lin, G.V. Selby, F.G. Howard, Exploratory Study of Vortex-Generating Devices for Turbulent Flow Separation Control, AIAA Pap, 1991.
[5] F.K. Lu, Q. Li, Y. Shih, A.J. Pierce, C. Liu, Review of Micro Vortex Generators in High-Speed Flow, 49th AIAA Aerosp. Sci. Meet., 2011, pp. 2011–2031.
[6] H.D. Taylor, Summary Report on Vortex Generators, United Aircraft Corporation. Research Dept., 1950.
[7] G.B. Schubauer, W.G. Spangenberg, Forced mixing in boundary layers, J. Fluid Mech. 8 (1959), https://doi.org/10.1017/s0022112060000372.
[8] H.H. Pearcey, Shock induced separation and its prevention by design and boundary layer control, in: G.V. Lachmann (Ed.), Bound. Layer Flow Control, vol. 2, Pergamon Press, 1961, pp. 1166–1344.
[9] J.C. Lin, Review of research on low-profile vortex generators to control boundary-layer separation, Prog. Aero. Sci. 38 (2002) 389–420, https://doi.org/10.1016/s0376-0421(02)00010-6.
[10] B. Wendt, B.A. Reichert, J.D. Foster, The Decay of Longitudinal Vortices Shed from Airfoil Vortex Generators, 1995.
[11] G. Godard, M. Stanislas, Control of a decelerating boundary layer. Part 1: optimization of passive vortex generators, Aero. Sci. Technol. 10 (2006) 181–191, https://doi.org/10.1016/j.ast.2005.11.007.
[12] D. Baldacchino, C. Ferreira, D. De Tavernier, W.A. Timmer, G.J.W. van Bussel, Experimental parameter study for passive vortex generators on a 30% thick airfoil, Wind Energy 21 (2018) 745–765, https://doi.org/10.1002/we.2191.
[13] D. Baldacchino, M. Manolesos, C. Ferreira, González Salcedo Á, M. Aparicio, T. Chaviaropoulos, et al., Experimental benchmark and code validation for airfoils equipped with passive vortex generators, J Phys Conf Ser 753 (2016), 022002, https://doi.org/10.1088/1742-6596/753/2/022002.
[14] K. Langan, J. Samuels, Experimental Investigation of Maneuver Performance Enhancements on an Advanced Fighter/attack Aircraft. 33rd Aerosp. Sci. Meet. Exhib, American Institute of Aeronautics and Astronautics, Reston, Virigina, 1995, p. 442, https://doi.org/10.2514/6.1995-442.
[15] J.-L. Aider, J.-F. Beaudoin, J.E. Wesfreid, Drag and lift reduction of a 3D bluff-body using active vortex generators, Exp. Fluid 48 (2009) 771–789, https://doi.org/10.1007/s00348-009-0770-y.
[16] A. Holmes, P. Hickey, W. Murphy, D. Hilton, The Application of Sub-boundary Layer Vortex Generators to Reduce Canopy "Mach Rumble" Interior Noise on the Gulfstream III. 25th AIAA Aerosp. Sci. Meet, American Institute of Aeronautics and Astronautics, Reston, Virigina, 1987, https://doi.org/10.2514/6.1987-84.
[17] R. Soto-Valle, S. Bartholomay, C.N. Nayeri, C.O. Paschereit, M. Manolesos, Airfoil Shaped Vortex Generators Applied on a Research Wind Turbine. AIAA Scitech 2021 Forum, American Institute of Aeronautics and Astronautics, Reston, Virginia, 2021, p. 1413, https://doi.org/10.2514/6.2021-1413.
[18] J. Alber, M. Manolesos, G. Weinzierl, A. Schönmeier, C.N. Nayeri, C.O. Paschereit, et al., Experimental Investigation of Mini-Gurney Flaps in Combination with Vortex Generators for Aerodynamic Improvements of Wind Turbine Blades. Wind Energy Sci. Conf. - EAWE, EAWE, Hannover, Germany, 2021.
[19] S. Øye, The Effect of Vortex Generators on the Performance of the ELKRAFT 1000 kW Turbine 9th IEA Symp, 9th IEA Symp. Aerodyn. Wind Turbines, Stockholm, 1995.
[20] H. Hwangbo, Y. Ding, O. Eisele, G. Weinzierl, U. Lang, G. Pechlivanoglou, Quantifying the effect of vortex generator installation on wind power production: an academia-industry case study, Renew. Energy 113 (2017) 1589–1597, https://doi.org/10.1016/j.renene.2017.07.009.
[21] W. Skrzypiński, M. Gaunaa, C. Bak, The effect of mounting vortex generators on the dtu 10mw reference wind turbine blade, J. Phys. Conf. Ser. 524 (2014), 12034, https://doi.org/10.1088/1742-6596/524/1/012034. IOP Publishing.

[22] G. Thomas Scarlett, I.M. Viola, Unsteady hydrodynamics of tidal turbine blades, Renew. Energy 146 (2020) 843–855, https://doi.org/10.1016/j.renene.2019.06.153.
[23] I. Afgan, J. McNaughton, S. Rolfo, D.D. Apsley, T. Stallard, P. Stansby, Turbulent flow and loading on a tidal stream turbine by LES and RANS, Int. J. Heat Fluid Flow 43 (2013) 96–108, https://doi.org/10.1016/j.ijheatfluidflow.2013.03.010.
[24] P. Kundu, A. Sarkar, V. Nagarajan, Improvement of performance of S1210 hydrofoil with vortex generators and modified trailing edge, Renew. Energy 142 (2019) 643–657, https://doi.org/10.1016/j.renene.2019.04.148.
[25] H. Singh, N. Kaufmann, P. Ouro, G. Papadakis, M. Manolesos, N. Kaufmann, et al., On the Use of Vortex Generators to Improve the Performance of Tidal Turbine Hydrofoils. Eur. Wave Tidal Energy Conf. - EWTEC, EWTEC, Plymouth, UK, 2021, p. 2026, 1-2026–9.
[26] N. Kaufmann, T.H. Carolus, R. Starzmann, An enhanced and validated performance and cavitation prediction model for horizontal axis tidal turbines, Int J Mar Energy 19 (2017) 145–163, https://doi.org/10.1016/j.ijome.2017.07.003.
[27] J.B. Barlow, W.H. Rae, A. Pope, Low-speed Wind Tunnel Testing, John Wiley & Sons, New York, 1999.
[28] M. Manolesos, S.G. Voutsinas, Experimental investigation of the flow past passive vortex generators on an airfoil experiencing three-dimensional separation, J. Wind Eng. Ind. Aerod. 142 (2015) 130–148, https://doi.org/10.1016/j.jweia.2015.03.020.
[29] L. Ch'ng, Using Vortex Generators and Gurney Flaps for Tidal Turbine Performance, Cranfield University, 2021.
[30] M. Drela, XFOIL: an analysis and design system for low Reynolds number airfoils, in: T.J. Mueller (Ed.), Low Reynolds Number Aerodyn, vol. 54, Springer-Verlag, NY, US, 1989, pp. 1–12.
[31] F.M. White, J. Majdalani, Viscous Fluid Flow, vol. 3, McGraw-Hill, New York, 2006.
[32] M. Drela, M.B. Giles, Viscous-inviscid analysis of transonic and low Reynolds number airfoils, AIAA J. 25 (1987) 1347–1355.
[33] G. Papadakis, Development of a Hybrid Compressible Vortex Particle Method and Application to External Problems Including Helicopter Flows, National Technical University of Athens, 2014.
[34] M. Manolesos, G. Papadakis, S.G.G. Voutsinas, Revisiting the assumptions and implementation details of the BAY model for vortex generator flows, Renew. Energy 146 (2020) 1249–1261, https://doi.org/10.1016/j.renene.2019.07.063.
[35] M. Manolesos, N.N. Sørensen, N. Troldborg, L. Florentie, G. Papadakis, S. Voutsinas, Computing the flow past vortex generators: comparison between RANS simulations and experiments, J Phys Conf Ser 753 (2016), 022014, https://doi.org/10.1088/1742-6596/753/2/022014.
[36] M. Manolesos, G. Papadakis, S.G. Voutsinas, Assessment of the CFD capabilities to predict aerodynamic flows in presence of VG arrays, J Phys Conf Ser 524 (2014), 012029, https://doi.org/10.1088/1742-6596/524/1/012029.
[37] F.R. Menter, Two-equation eddy-viscosity turbulence models for engineering applications, AIAA J. 32 (1994) 1598–1605, https://doi.org/10.2514/3.12149.
[38] A. Jirasek, Vortex-generator model and its application to flow control, J. Aircraft 42 (2005) 1486–1491, https://doi.org/10.2514/1.12220.
[39] L. Chng, L. Alber, D. Ntouras, G. Papadakis, N. Kaufmann, P. Ouro, et al., On the Combined Use of Vortex Generators and Gurney Flaps for Turbine Airfoils, J. Phys. Conf. Ser., Delft, the Netherlands, 2022.
[40] M. Manolesos, G. Papadakis, S.G. Voutsinas, Experimental and computational analysis of stall cells on rectangular wings, Wind Energy 17 (2014) 939–955, https://doi.org/10.1002/we.1609.
[41] M. Manolesos, Experimental and Computational Study of Three-Dimensional Separation and Separation Control Using Passive Vortex Generators, National Technical University of Athens, 2013.
[42] C. Lindenburg, Investigation into Rotor Blade Aerodynamics, Energy Res Cent Netherlands Wind Energy Publ ECN-C–03-025, 2003.
[43] A. Gross, H. Fasel, T. Friederich, M. Kloker, Numerical Investigation of S822 Wind Turbine Airfoil, 40th Fluid Dyn. Conf. Exhib., 2010, p. 4478.
[44] N. Troldborg, F. Zahle, N.N. Sørensen, Simulations of wind turbine rotor with vortex generators, in: J. Phys. Conf. Ser., vol. 753, IOP Publishing, 2016, 22057.
[45] M. Lewis, S.P. Neill, P. Robins, M.R. Hashemi, S. Ward, Characteristics of the velocity profile at tidal-stream energy sites, Renew. Energy 114 (2017) 258–272.
[46] B. Gaurier, G. Germain, J.V. Facq, C.M. Johnstone, A.D. Grant, A.H. Day, et al., Tidal energy "Round Robin" tests comparisons between towing tank and circulating tank results, Int J Mar Energy 12 (2015) 87–109, https://doi.org/10.1016/j.ijome.2015.05.005.
[47] C. Bak, W. Skrzypiński, M. Gaunaa, H. Villanueva, N.F. Brønnum, E.K. Kruse, Full scale wind turbine test of vortex generators mounted on the entire blade, in: J. Phys. Conf. Ser., vol. 753, IOP Publishing, 2016, 22001.